Research Journal of Applied Sciences, Engineering and Technology 8(18): 1966-1972, 2014
DOI:10.19026/rjaset.8.1188
ISSN: 2040-7459; e-ISSN: 2040-7467
© 2014 Maxwell Scientific Publication Corp.
Submitted: August 19, 2014 Accepted: September 13, 2014 Published: November 15, 2014

**Research Article**

# An Adapted Block Thresholding Method for Omnidirectional Image Denoising

[1]Brahim Alibouch, [1]Abderrazak Iazzi, [2]Amina Radgui and [1]Mohammed Rziza
[1]LRIT Associated Unit with CNRST (URAC29), Mohammed V-Agdal University, B.P. 1014,
[2]INPT, Madinat AL Irfane, Rabat, Morocco

**Abstract:** The problem of image denoising is largely discussed in the literature. It is a fundamental preprocessing task, and an important step in almost all image processing applications. Omnidirectional images offer a large field of view compared to conventional perspectives images, however, they contain important distortions and classical treatments are thus not appropriate for those deformed omnidirectional images. In this study we introduce an adaptation of an adaptation to Stein block thresholding method to omnidirectional images. We will adapt different treatments in order to take into account the nature of omnidirectional images.

**Keywords:** Block thresholding, image denoising, omnidirectional image, wavelet

## INTRODUCTION

Image denoising is a basic problem in image processing. It represents an important task in almost all image processing applications. It is defined as the process of removing unwanted noise in order to restore the original image. Among all image denoising techniques, wavelet based methods are known to yield the best results. This is due to their excellent localization property which became an indispensable signal and image processing tool to many image processing of application since it provides an appropriate basis for separation noisy signal from the image signal.

Over the last two decades several methods were proposed for image denoising using wavelet thresholding. These techniques can be grouped in two classes: individually thresholding (Donoho and Johnstone, 1994; Donoho, 1995; Chang *et al*., 2000; Kalavathy and Suresh, 2011) and block thresholding (Efroimovich, 1986; Kerkyacharian *et al*., 1996; Cai, 1997, 1999, 2002; Cai and Zhou, 2009). Unlike perspective images, omnidirectional images offer a large field of view. However they present a non-uniform resolution and important geometric distortions. Figure 1 shows an example of omnidirectional sensor.

Recently, several works have been interested in the denoising problem for omnidirectional images. Bigot-Marchand (2008) used the sphere as a projection space for omnidirectional images and defined image processing tools in that space in order to perform the image denoising. Demonceaux and Vasseur (2006) used Markov Random Fields and defined an adapted system neighborhood for omnidirectional images.

Fig. 1: An omnidirectional sensor mounted on mobile robot and the obtained omnidirectional image

In this study, we will adapt the Stein block thresholding algorithm to omnidirectional images. The remainder of the study is as follows: In the next section we present the Stein block thresholding approach for perspective images denoising (Chesneau *et al*., 2010).

**Stein block thresholding for perspective images denoising:** Let's consider the nonparametric regression model:

$$Y = X + \sigma\varepsilon \tag{1}$$

where, $X = (X_{(n,m)})_{(n,m)}$ is the noiseless image, $Y = (y_{(n,m)})_{(n,m)}$ is the noisy image, $\varepsilon = (\varepsilon_{(n,m)})_{(n,m)}$ are i.i.d, $n$, $m = 1,\ldots,N$. The aim is to denoise Y by finding an estimate X of the noiseless image X that minimize the mean squared error.

Let $Y_{j,\ell,k}$, $\theta_{j,\ell,k} = \langle X, \psi_{j,\ell,k}\rangle$ and $Z_{j,\ell,k} = \langle \varepsilon, \psi_{j,\ell,k}\rangle$ denote, respectively, the matrix of wavelet coefficients

**Corresponding Author:** Brahim Alibouch, LRIT Associated Unit with CNRST (URAC29), Mohammed V-Agdal University, B.P. 1014, Rabat, Morocco
This work is licensed under a Creative Commons Attribution 4.0 International License (URL: http://creativecommons.org/licenses/by/4.0/).

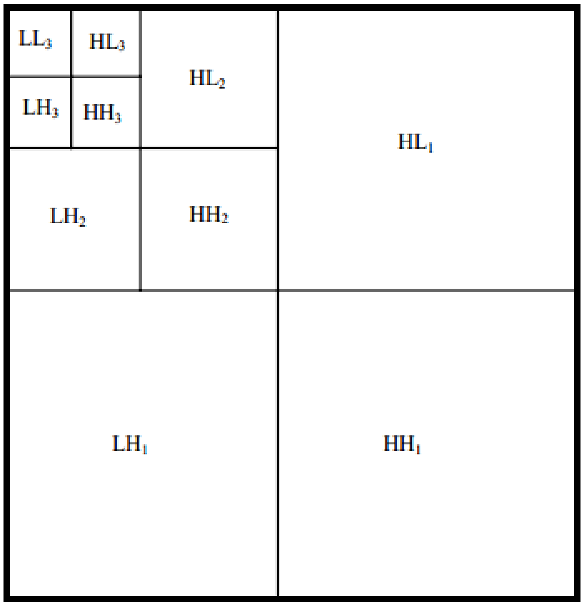


Fig. 2: Subbands of 2-D orthogonal wavelet transform

of Y, the matrix of Unknown coefficients and a sequence of noise random variables, where $\psi_{j,l,k}$ is the two-dimensional dyadic orthogonal wavelet transform operator, $j = \{0, ..., J\}$ is the scale parameter, $J = \log_{10} N$, $\ell \in \{1, 2, 3\}$ is a generic integer indexing of subband, $k \in D_j = \prod_{i=1}^{2} \{0, ..., 2^j - 1\}$ is the position parameters.
The observed sequence of coefficients is defined by:

$$Y_{j,\ell,\mathrm{k}} = \theta_{j,\ell,\mathrm{k}} + \sigma Z_{j,\ell,k} \quad (2)$$

Figure 2 shows a representation of the Wavelet Transform. The subbands $HH_j$, $HL_j$ and $LH_j$ are called the details. The subband $LL_j$ is the low resolution residual.

The block thresholding methods was proposed in Hall *et al*. (1999) and developed, generalized to any dimension and applied to image denoising in Chesneau *et al*. (2010). The main of this method is to increase the quality of estimation by using the neighborhood information of the wavelet coefficients. The procedure first divides the wavelet coefficients at each resolution level into non-overlapping blocks and then keeps all the coefficients within a block if and only if, the magnitude of the sum of the squared empirical coefficients within that block is greater than a fixed threshold (Chesneau *et al*., 2010).

Let $A_j = \{1, ..., 2^j L^{-1}\}$ be the set indexing the blocks at scale j where L is the block length. For each block index $K \in A_j$, let $B_{j,k}$ be the set indexing the position of coefficients within the $K^{th}$ block:

$$B_{j,K} = \left\{ (x, y); (K-1)L + 1 \le x \le KL \text{ and } 1 \le y \le \frac{n}{2^j} \right\} \quad (3)$$

The rule of shrinkage of James-stein at block Eq. (3):

$$\hat{\theta}_{j,\ell,k} = \begin{cases} y_{j,\ell,k} \left(1 - \frac{\lambda_* \sigma^2}{L^{-2} \sum_{k \in B_{j,K}} y_{j,\ell,k}^2}\right)_+ & j \in \{0, ..., J\} \\ 0 & \text{Otherwise} \end{cases} \quad (4)$$

where $\lambda_*$ is the threshold. For each block $B_{j,K}$ at scale $j = \{0, ..., J\}$ if the mean energy within the block $L^{-2} \sum_{k \in B_{j,K}} y_{j,\ell,k}^2$ is larger than $\lambda_* \sigma$ then $y_{j,\ell,k}$ is shrunk by the amount:

$$y_{j,\ell,k} \frac{\lambda_* \sigma^2}{L^{-2} \sum_{k \in B_{j,K}} y_{j,\ell,k}^2}$$

Otherwise $\hat{\theta}_{j,\ell,k}$ is estimated by zero (Chesneau *et al*., 2010).

## ADAPTED METHOD FOR OMNIDIRECTIONAL IMAGES

Omnidirectional images offer a large field of view, nevertheless, they contains significant radial distortions and present non-uniform resolution due to the non-linear projection. Consequently, denoising such images in the same way as a perspective image will lead to mistaken results. In the literature there are two ways to treat omnidirectional images. One is treating them such as perspective images by adapting their characteristic. The other, is to use the projection on the sphere and perform all treatments in this domain.

**Stereographic projection:** Geyer and Daniilidis (2000) introduced the unifying theory for all central catadioptric sensors. They prove that the central catadioptric projection is equivalent to a central

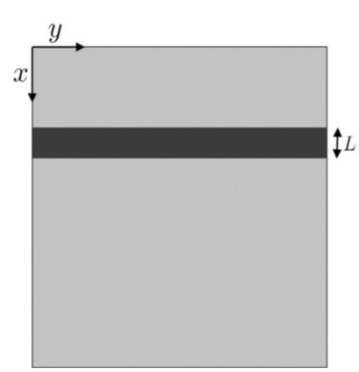


Fig. 3: Representation of a block as defined by Eq. (3)

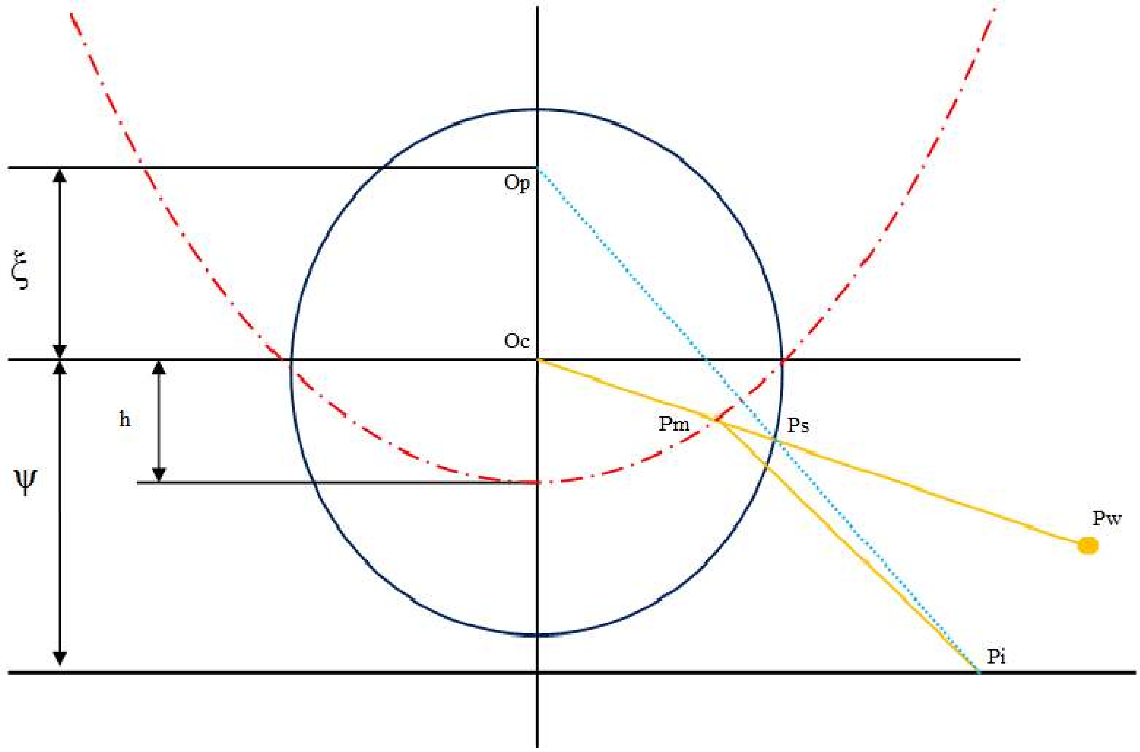


Fig. 4: Equivalence between the catadioptric projection and the two step mapping via the sphere

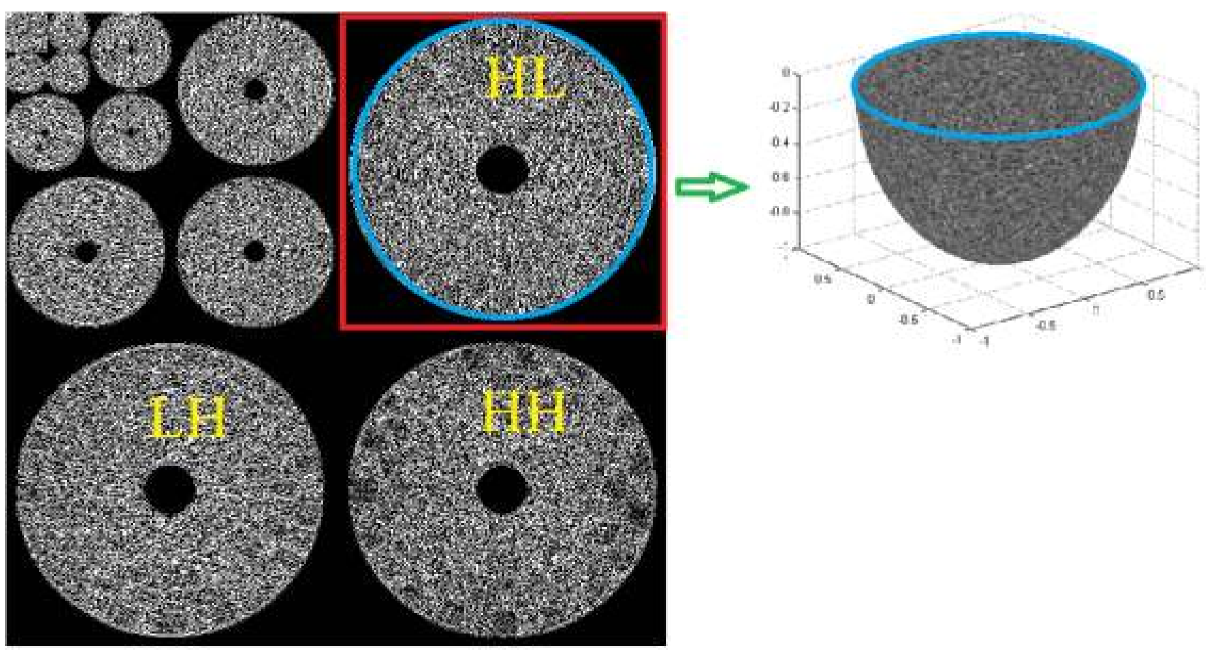


Fig. 5: The subband of DWT (left) subband projection to hemi-sphere (right)

projection to a virtual sphere followed by a projection from the sphere to the retina. This second projection depends on the shape of the mirror. Figure 3 and 4 shows the equivalence between the catadioptric projection and the two step mapping via the sphere.

The parameter $\xi$ defines the shape of mirror. In our case, we consider parabolic mirror where $\xi = 1$. However, the method can easily be adapted to the general case, let $P_s(\theta,\varphi) = P_s(X_s, Y_s, Z_s)$ be the point on the sphere. The Cartesian coordinates of this point are given by:

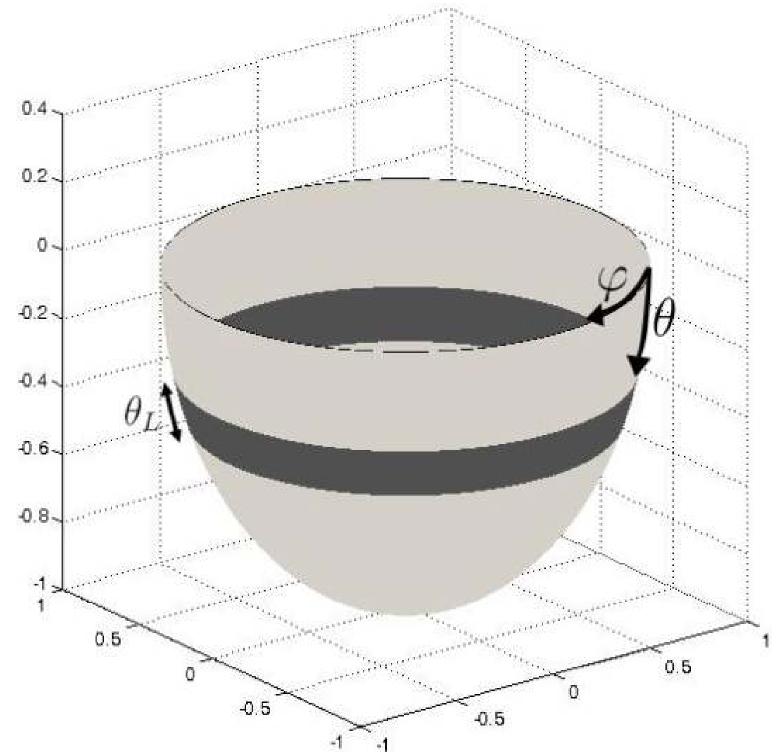


Fig. 6: Representation of the spherical block as defined in Eq. (8)

$$\begin{cases} X = \cos\varphi \sin\theta \\ Y = \sin\varphi \sin\theta \\ Z = \cos\theta \end{cases} \tag{5}$$

The stereographic projection of $P_s$ on the image plane yields point $P_i$ (x, y) given by:

$$\begin{cases} x = \dfrac{X_s}{1-Z_s} \\ y = \dfrac{Y_s}{1-Z_s} \end{cases} \tag{6}$$

By combining Eq. (5) and (6) we obtain the spherical coordinates of point $P_i$:

$$\begin{cases} x = \cot(\dfrac{\theta}{2})\cos\varphi \\ \mathrm{y} = \cot(\dfrac{\theta}{2})\sin\varphi \end{cases} \tag{7}$$

**Adapted spherical block estimator:** The block as defined in the classic stein block thresholding method has the shape of a rectangle. In our case we need to define the block in the sphere in order to take into account the radial distortions present in omnidirectional images. Each subband is mapped on the sphere (Fig. 5) and a spherical block is defined according to the spherical coordinates $\theta$ and $\varphi$ as shown in Fig. 6.

The set indexing the position of coefficients within the K[th] block in the sphere is defined by:

$$Us_{j,K} = \left\{(\theta,\varphi), 0 \le \varphi \le 2\pi \text{ and } \frac{\pi}{2} + (K-1)\theta_L \frac{\pi}{2n} \le \theta \le \frac{\pi}{2} + K\theta_L \frac{\pi}{2n}\right\} \tag{8}$$

where $\theta_L$ is the block length, $A_j = \left\{1,\ldots,2^j(\theta_L)^{-1}\right\}$ is the set indexing the blocks in the sphere at scale j.

The suitable estimator for omnidirectional images is given using the Stereographic Projection:

$$\hat{\theta}_{j,\ell,k} = \begin{cases} y_{j,\ell,k}\left(1 - \dfrac{\lambda_* \sigma^2}{L^{-2} \sum\limits_{k \in Up_{j,K}} y^2_{j,\ell,k}}\right)_+ & j \in \{0,\ldots,J\} \\ 0 & \text{Otherwise} \end{cases} \tag{9}$$

where $U_p$ is the spherical block as defined in Eq. (8) for omnidirectional images.

## APPLICATION AND RESULTS

To show the improvement given by our proposed adapted method, we have applied it on synthetic omnidirectional images of 512*512 pixels obtained using the ray tracing program POV-Ray. We created a scene where a parabolic camera, initially at the origin of the three dimensional Cartesian coordinate system and looking in the y-axis. This camera observes two planes

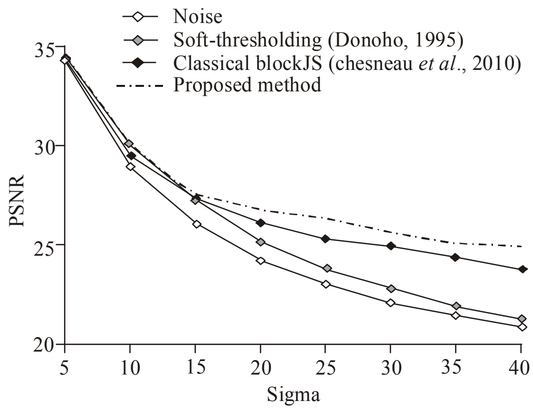


Fig. 7: Comparison of PSNR evolution against the noise level for different image denoising methods on synthetic image

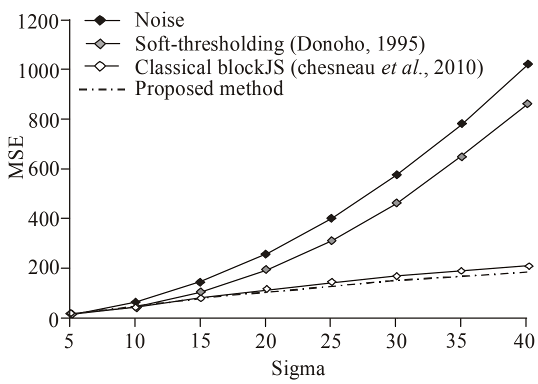


Fig. 8: Comparison of MSE evolution against the noise level for different image denoising methods on synthetic image

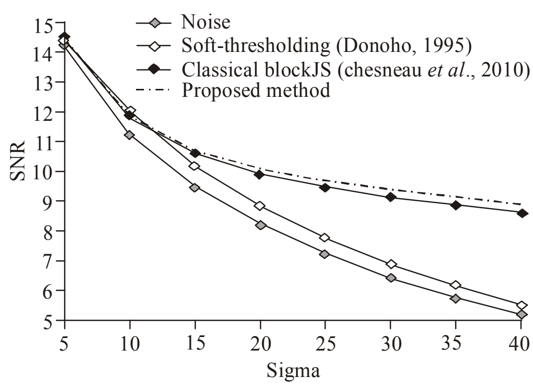


Fig. 9: Comparison of SNR evolution against the noise level for different image denoising methods on synthetic image

at the same distance of the origin and parallel to yz-plane. These images are corrupted by different levels of additive white Gaussian noises $\sigma$ = (5, 10, 15, 20, 25, 30, 35, 40). As in Chesneau *et al*. (2010), we used a block size L = 4 and a threshold $\lambda = 4.5$.

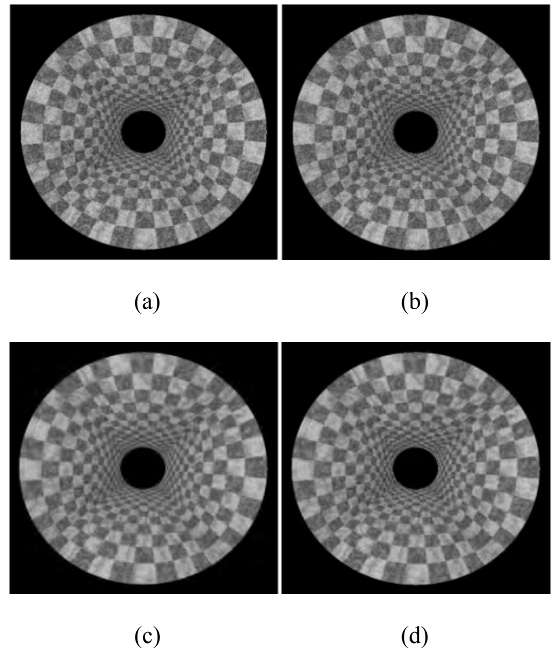


Fig. 10: Visual comparison of denoising methods on synthetic image (a) noisy $\sigma = 30$, (b), (c) and (d) denoising using respectively the soft-thresholding method (Donoho, 1995), the classical Stein block thresholding method result of denoising methods (Chesneau *et al*., 2010) and our proposed method

We have compared our results with the classical method proposed in Chesneau *et al*. (2010) and with the soft-thresholding method proposed in Donoho (1995). We have applied the orthogonal wavelet transform to get the wavelet coefficients using the Symmlet wavelet with 6 order vanishing moments.

In order to measure methods performances we calculate the Peak Signal to Noise Ratio (PSNR), the Mean Square Error (MSE) and the Signal to Noise Ratio (SNR) given by:

$$PSNR = 10\log_{10}\frac{max(f)^2}{MSE} \tag{10}$$

$$SNR = 10\log_{10}\frac{norm(f)}{MSE} \tag{11}$$

$$MSE = \mathrm{E}\left(\left\|f - \hat{f}\right\|^2\right) \tag{12}$$

where $f$ and $\hat{f}$ are respectively the reference and the denoised image.

Figure 7 and 8 respectively show the evolution of the PSNR and the SNR against the noise level. Overall, both the PSNR and the SNR values of our proposed approach remain higher than those for the other two methods. The evolution of the MSE against the noise level is displayed in Fig. 9 and 10 shows a visual

Table 1: PSNR evolution against the noise level for different image denoising methods on real image

| | 10 | 20 | 30 | 40 |
|---|---|---|---|---|
| Noise | 31.3507 | 26.4295 | 23.8834 | 22.2617 |
| Soft-thresholding (Donoho, 1995) | 33.1495 | 27.4372 | 24.5298 | 22.7205 |
| Classical blockJS (Chesneau *et al*., 2010) | 34.6340 | 30.5891 | 28.5212 | 27.3093 |
| Proposed method | 34.8089 | 31.2183 | 29.3155 | 27.9670 |

Table 2: SNR evolution against the noise level for different image denoising methods on real image

| | 10 | 20 | 30 | 40 |
|---|---|---|---|---|
| Noise | 10.4708 | 7.46048 | 5.69957 | 4.45018 |
| Soft-thresholding (Donoho, 1995) | 11.5508 | 8.13632 | 6.17621 | 4.81686 |
| Classical blockJS (Chesneau *et al*., 2010) | 12.2542 | 10.03050 | 8.87319 | 8.12887 |
| Proposed method | 12.3713 | 10.23020 | 9.11607 | 8.38710 |

Table 3: MSE evolution against the noise level for different image denoising methods on real image

| | 10 | 20 | 30 | 40 |
|---|---|---|---|---|
| Noise | 63.665574 | 254.66230 | 572.99017 | 1018.6492 |
| Soft-thresholding (Donoho, 1995) | 43.913260 | 191.04300 | 463.26880 | 862.4754 |
| Classical blockJS (Chesneau *et al*., 2010) | 35.201790 | 94.95507 | 161.66690 | 226.9943 |
| Proposed method | 34.272860 | 93.18572 | 155.11100 | 215.1497 |

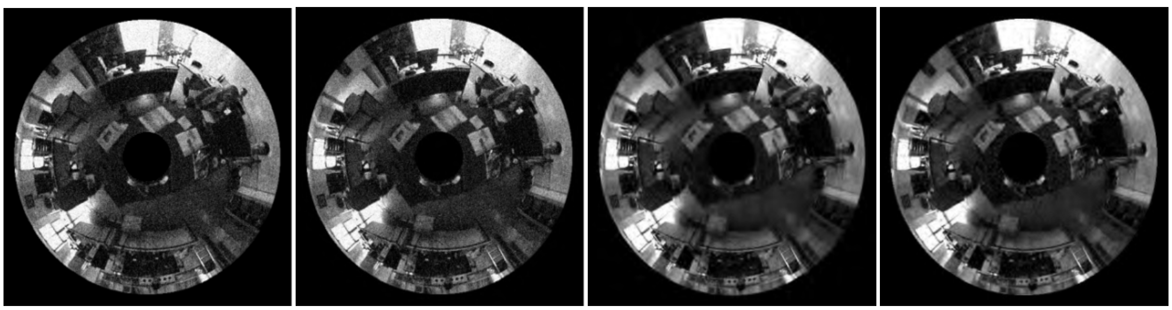

(a) (b) (c) (d)

Fig. 11: Visual comparison of denoising methods on real image (a) noisy $\sigma = 30$ , (b), (c) and (d) denoising using respectively the soft-thresholding method (Donoho, 1995), the classical stein block thresholding method result of denoising methods (Chesneau *et al*., 2010) and our proposed method

comparison of denoising results obtained by different methods using the same noise level $\sigma = 30$ . It can be seen that our method achieves the smallest values of MSE compared with the other two methods.

We used also real omnidirectional images. They are captured using a catadioptric camera embedded on a mobile robot as shown in Fig. 1. Table 1 to 3 shows, respectively, the evolution of the PSNR, the SNR and the MSE against the noise level. Figure 11 shows a visual comparison of denoising results obtained by different methods using the same noise level $\sigma = 30$ . These results confirm the previous positive results obtained on synthetic images and show that the classical approaches (Donoho, 1995; Chesneau *et al*., 2010), even if these methods work well for perspectives images, are not appropriate to omnidirectional images.

## CONCLUSION

Omnidirectional images are rich in information since they depict almost the whole scene. Unfortunately, they include severe distortions. That is why classical image denoising techniques that work for perspectives images need to be adapted for omnidirectional ones.

In this study we have proposed an adaptation to Stein block thresholding (Chesneau *et al*., 2010). We applied our approach in synthetic and real images and we compared it to the classical methods (Donoho, 1995; Chesneau *et al*., 2010). The comparison shows that our adapted method has the best overall results over any other method.

## REFERENCES


Bigot-Marchand, S., 2008. Outils de traitement d'images adaptés au traitement d'images omnidirectionnelles. Ph.D. Thesis, Department of Mathematics, University of Picardie Jules Verne, Amiens.

Cai, T.T., 1997. On adaptivity of blockshrink wavelet estimator over besov spaces. Technical Report 97-05, Purdue University.

Cai, T.T., 1999. Adaptive wavelet estimation: a block thresholding and oracle inequality approach. Ann. Stat., 27(3): 898-924.

Cai, T.T., 2002. On block thresholding in wavelet regression: Adaptivity, block size, and threshold level. Stat. Sinica, 12(4): 1241-1274.

Cai, T.T. and H.H. Zhou, 2009. A data-driven block thresholding approach to wavelet estimation. Ann. Stat., 37(2): 569-595.

Chang, S.G., B. Yu and M. Vetterli, 2000.Adaptive wavelet thresholding for image denoising and compression. IEEE T. Image Process., 9(9): 1532-1546.

Chesneau, C., J. Fadili and J.L. Starck, 2010. Stein block thresholding for image denoising. Appl. Comput. Harmon. A., 28(1): 67-88.

Demonceaux, C. and P. Vasseur, 2006. Markov random fields for catadioptric image processing. Pattern Recogn. Lett., 27(16): 1957-1967.

Donoho, D.L., 1995. De-noising by soft-thresholding. IEEE T. Inform. Theory, 41(3): 613-627.

Donoho, D.L. and J.M. Johnstone, 1994. Ideal spatial adaptation by wavelet shrinkage. Biometrika, 81(3): 425-455.

Efroimovich, S.Y., 1986. Nonparametric estimation of a density of unknown smoothness. Theor. Probab. Appl+., 30(3): 557-568.

Geyer, C. and K. Daniilidis, 2000. A unifying theory for central panoramic systems and practical implications. Proceeding of the 6th European Conference on Computer Vision (Computer Vision-ECCV'2000). Dublin, Ireland, pp: 445-461.

Hall, P., G. Kerkyacharian and D. Picard, 1999. On the minimax optimality of block thresholded wavelet estimators. Stat. Sinica, 9(1): 33-49.

Kalavathy, S. and R.M. Suresh, 2011. Analysis of image denoising using wavelet coefficient and adaptive subband thresholding technique. Int. J. Comput. Sci., 8(1): 166-172.

Kerkyacharian, G., D. Picard and K. Tribouley, 1996. Lp adaptive density estimation. Bernoulli, 2(3): 229-247.